Magnetized black holes with anisotropic matter: degeneracy with the Kerr spin in the ISCO radius and radiative efficiency

Munisa Boltatoshova[1†] Bakhtiyor Narzilloev[1‡] Ibrar Hussain[2§] Bobomurat Ahmedov[1,3,4¶]

[1]Institute for Advanced Studies, New Uzbekistan University, Movarounnahr str. 1, Tashkent 100000, Uzbekistan
[2]School of Electrical Engineering and Computer Science, National University of Sciences and Technology, H-12, Islamabad, Pakistan
[3]School of Physics, Harbin Institute of Technology, Harbin 150001, People's Republic of China
[4]Institute of Theoretical Physics, National University of Uzbekistan, Tashkent 100174, Uzbekistan

Abstract: We investigate the dynamics of charged test particles around a static black hole surrounded by anisotropic matter and immersed in an external, asymptotically uniform magnetic field. Using the Hamilton–Jacobi formalism, we analyze circular orbits, the structure of the effective potential, innermost stable circular orbits (ISCOs), and radiative efficiency, explicitly accounting for the effects of the anisotropy parameter K, the equation-of-state parameter ω, and the magnetic coupling parameter Ω_B. Our results show that anisotropic matter primarily modifies the background geometry, generally shifting the ISCO outward and weakening orbital binding. However, radiation-dominated matter ($\omega = 1/3$) yields smaller ISCO radii than the dust case. In contrast, the external magnetic field plays a dominant dynamical role: negative values of Ω_B significantly enhance gravitational binding, move the ISCO closer to the horizon, and increase the radiative efficiency to values comparable to those of rapidly rotating Kerr black holes. By constructing degeneracy maps based on the ISCO radius and radiative efficiency, we demonstrate that non-rotating magnetized black holes surrounded by anisotropic matter can reproduce the ISCO radius and the corresponding ISCO-based radiative efficiency of spinning Kerr black holes, two quantities that enter X-ray continuum-spectrum fitting. This degeneracy is restricted to these ISCO-based quantities and does not imply equivalence with the full phenomenology of the Kerr spacetime.

Keywords: Magnetized black holes, anisotropic matter, Kerr black hole

DOI: 10.1088/1674-1137/aeb48c **CSTR:**

CPC Accepted

I. INTRODUCTION

The standard theory describing the gravitational interaction, known as General Relativity (GR), was proposed by Albert Einstein in 1915 and remains the most widely accepted theory of gravity to date. The basic equations of GR, known as the Einstein field equations, admit singular solutions called black hole solutions, which are an intriguing feature of Einstein's theory. Following the observations of supermassive black holes at the centers of the galaxies M87 and the Milky Way [1, 2], their existence is no longer in doubt, motivating researchers to study such objects in greater detail. Black holes can be regarded as laboratories for testing theories of gravity by studying various features of null and timelike geodesics, including shadows, gravitational lensing, quasi-periodic oscillations, and quasi-normal modes in their vicinity [1, 3–9].

Due to gravitational attraction near black hole horizons and the effects of radiation reaction, ordinary matter may not remain in equilibrium with black holes. However, when quantum effects such as Hawking radiation are taken into account, an equilibrium system may be possible. There are well-known examples in which matter remains stably distributed around a black hole [10]. For instance, for the Reissner-Nordström black hole solution, the stress-energy tensor of the electromagnetic field outside the black hole is anisotropic [11]. Cho and Kim [12] studied a black hole solution involving an anisotropic matter field with negative pressure, in which the energy density vanishes at the event horizon. Considering the significance of anisotropic fluids in the study of traversable wormholes and static matter configurations [13], Cho and Kim analyzed black hole solutions of the Einstein field equations incorporating negative pressure and anisotropic fluid configurations. They found exact black hole solutions with anisotropic matter character-

Received 16 March 2026; Accepted 14 October 2026

† E-mail: m.boltatoshova@newuu.uz
‡ E-mail: b.narzilloev@newuu.uz
§ E-mail: ibrar.hussain@seecs.nust.edu.pk
¶ E-mail: ahmedov@astrin.uz

©2026 Chinese Physical Society and the Institute of High Energy Physics of the Chinese Academy of Sciences and the Institute of Modern Physics of the Chinese Academy of Sciences and IOP Publishing Ltd. All rights, including for text and data mining, AI training, and similar technologies, are reserved.

ized by two parameters [12]. Their black hole solution with an anisotropic fluid has also been analyzed in the presence of rotation and within the framework of modified theories of gravity [14–16]. Furthermore, particle dynamics and related phenomena associated with the Cho and Kim black hole have been explored in the literature [17–20].

According to the no-hair theorem, black holes can be fully characterized by only three parameters: mass, electric charge, and angular momentum (spin). As a result, black holes themselves cannot produce intrinsic magnetic fields. However, magnetic fields can arise in the vicinity of black holes due to the motion of charged particles in the surrounding accretion disk. Another possible source of external magnetic fields near black holes is the presence of nearby magnetars or neutron stars [21]. Synchrotron emission and polarization (SEP) from radio observations have provided valuable insights into the nature of magnetic fields in the interstellar medium, including regions between galaxies in the cosmos [22]. The existence of magnetic fields in the vicinity of astrophysical black holes has been reported in the literature [23], and observations indicate that Sgr A^* is surrounded by a strong magnetic field [24]. These findings have further stimulated interest in studying such scenarios in greater detail. Numerous studies in the literature have investigated various black hole spacetimes in the presence of external magnetic fields, focusing on different aspects such as the motion of null and timelike particles and the resulting astrophysical phenomena [25–38].

In this work, we aim to explore the black hole solution obtained by Cho and Kim [12, 39] with anisotropic matter in the presence of an asymptotically uniform magnetic field by analyzing the motion of test particles in its vicinity. Our goal is to probe the effects of the spacetime parameters and the external magnetic field on particle dynamics. Furthermore, we investigate whether the ISCO radius and radiative efficiency of the black hole with anisotropic matter can reproduce those of a Kerr black hole, following the approach adopted in Ref. [40]. A closely related degeneracy among the innermost stable circular orbit, radiative efficiency, and Kerr spin parameter has also been reported for other regular and charged black hole spacetimes [41]. This has significant astrophysical importance, as these quantities are the primary observables inferred from X-ray continuum-spectrum fitting [4].

This paper is organized as follows. In Sect. II, we introduce the black hole solution with anisotropic matter and the external magnetic field configuration. In Sect. III, we analyze the dynamics of charged particles, ISCO properties, and parameter degeneracies with Kerr rotation. The implications for radiative efficiency and observational signatures are discussed in detail. Finally, Sect. IV summarizes our main findings and outlines future prospects.

In this study, we employ geometrized units in which the gravitational constant and the speed of light are set to unity, $G = c = 1$. The spacetime metric is taken to have signature $(-,+,+,+)$, and Greek indices are used to label four-dimensional spacetime coordinates.

II. BLACK HOLE SURROUNDED BY FIELDS OF ANISOTROPIC MATTER

$$ds^2 = -f(r)dt^2 + f(r)^{-1}dr^2 + r^2(d\theta^2 + \sin^2\theta d\phi^2),$$
$$f(r) = 1 - \frac{2M}{r} - \frac{K}{r^{2\omega}}. \tag{1}$$

Here, M is the mass of the black hole, K is the anisotropy parameter, and ω is the equation-of-state parameter of the matter surrounding the black hole. The metric (1) describes a black hole surrounded by a generic matter field specified by an equation of state. In this paper, we investigate the cases of dust $(\omega = 0)$ and radiation $(\omega = 1/3)$. It can be readily verified that setting the parameter $K = 0$ recovers the standard Schwarzschild geometry.

It is worth noting that for $\omega = 0$, the metric function satisfies $f(r) \to 1 - K$ as $r \to \infty$, so the spacetime is not asymptotically flat unless $K = 0$; the constant K effectively rescales the asymptotic time coordinate. For $\omega = 1/3$, on the other hand, $f(r) \to 1$ as $r \to \infty$, and the spacetime is asymptotically flat. The normalization parameter K characterizes the strength of the anisotropic matter distribution: for $\omega = 0$, it is related to the effective matter energy density via $\rho \approx K/(8\pi M^2)$ in geometrized units, while for $\omega = 1/3$, it acts as a radiation-like normalization constant. Following the approach of Refs. [17, 19], we adopt $K \in [0, 0.1]$ as the primary physically motivated regime, which (I) ensures the existence of a well-defined event horizon, (II) maintains the subdominance of the matter sector for $\omega = 0$, and (III) allows us to explore a physically reasonable observational imprint of anisotropic matter on the orbital dynamics of test particles. In certain figures, we extend the range beyond the physically motivated regime solely to illustrate the qualitative robustness of the observed trends, up to $K = 0.35$ for $\omega = 0$ in Fig. 5 and up to $K = 0.18$ for $\omega = 1/3$ in Fig. 8. The quantitative astrophysical conclusions remain restricted to $K \in [0, 0.1]$ throughout.

Fig 1 illustrates the dependence of the horizon on the anisotropy parameter for two anisotropic matter configurations, corresponding to dust and radiation. The figure shows that, as K increases, the horizon in the radiation case remains systematically smaller than that in the dust case, demonstrating the sensitivity of the horizon structure to the parameter ω of the effective matter field.

Employing the Wald method [23], the electromagnet-

CPC Accepted

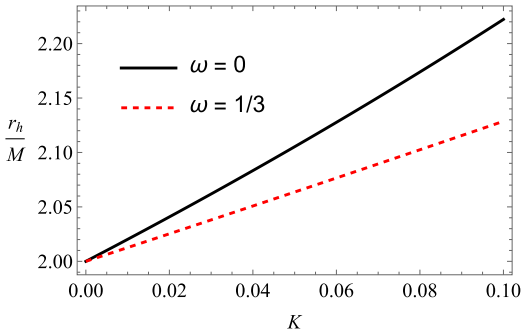


Fig. 1. (color online) Behavior of the event horizon radius as a function of the spacetime parameters K and ω.

ic four-potential A^μ for a black hole immersed in a uniform magnetic field is typically constructed as a linear combination of the Killing vectors, based on the vacuum identity

$$\xi^{\alpha}{}_{;\beta}{}^{;\beta} = -R^{\alpha}{}_{\gamma}\xi^{\gamma} = 0. \tag{2}$$

This identity does not hold in the present case because the metric (1) is sourced by anisotropic matter and is therefore not Ricci-flat; a direct computation yields

$$\begin{aligned} R^{t}{}_{t} &= R^{r}{}_{r} = K\omega(2\omega-1)\, r^{-2(1+\omega)}, \\ R^{\theta}{}_{\theta} &= R^{\varphi}{}_{\varphi} = -K(2\omega-1)\, r^{-2(1+\omega)}, \end{aligned} \tag{3}$$

which is nonzero for $K \neq 0$. Following Ref. [42], we solve the equation $\Box a^{\alpha} = \eta^{\alpha} \equiv R^{\alpha}{}_{\gamma}\xi^{\gamma}_{(\varphi)}$ for the correction to the axial component of the potential. We discard the contribution from the timelike Killing vector by imposing the condition that the net electric charge vanish at spatial infinity, as originally required by Wald [23]. This yields, for $\omega \neq 0$,

$$a^{\varphi}_{(\varphi)}(r) = -\frac{K(2\omega-1)}{2\omega(1+2\omega)}\, r^{-2\omega}, \tag{4}$$

and, consequently, the corrected test-field four-potential

$$A^{\mu} = \left(0,0,0,\ \frac{B}{2}\left(1+\frac{K(1-2\omega)}{2\omega(1+2\omega)}\, r^{-2\omega}\right)\right). \tag{5}$$

In the dust case $\omega = 0$, which is the main focus below, Eq.(5) is singular; the correct result is obtained by taking the limit $\omega \to 0$ before integration, yielding $\eta^{\varphi}_{(\varphi)} = K/r^2$ and

$$A^{\mu} = \left(0,0,0,\ \frac{B}{2}\left(1-K\log\frac{r}{M}\right)\right). \tag{6}$$

For the integration constant C in $a^{\varphi}_{(\varphi)}(r) = -K\ln r + C$, we instead set $C = K\ln M$, where M is the only length scale intrinsic to the metric (1) in geometrized units. This choice affects only the additive constant in A_φ and leaves the physical quantity $\eta^{\varphi}_{(\varphi)} = K/r^2$ unchanged.

From the metric, the corresponding covariant component is

$$A_{\varphi} = \begin{cases} \dfrac{1}{2}Br^2\sin^2\theta\left(1-\dfrac{K(2\omega-1)}{2\omega(1+2\omega)}\, r^{-2\omega}\right), & \omega \neq 0, \\ \dfrac{1}{2}Br^2\sin^2\theta\left(1-K\log\frac{r}{M}\right), & \omega = 0. \end{cases} \tag{7}$$

We emphasize that the two sectors of the model are treated at different levels. The gravitational sector is exact: the metric (1) is a solution of the Einstein equations sourced by the anisotropic fluid [12, 39]. By contrast, the electromagnetic field is treated as a test field. The four-potential (5)–(7) satisfies Maxwell's equations on this fixed background, including the correction required because the background is not Ricci-flat [42]; however, its stress–energy tensor is not included in the Einstein equations. Therefore, the magnetic field does not backreact on the geometry and affects only the motion of charged particles. In particular, the horizon radius (Fig. 1) does not depend on Ω_B. This approximation is well justified because the field would significantly alter the geometry only for $B \sim B_M = c^4/(G^{3/2}M) \simeq 2.4\times10^{19}\,(M_\odot/M)\,\mathrm{G}$. By contrast, $|\Omega_B| \sim 0.6$ corresponds to $B \sim 2.5\,\mathrm{G}$ for protons and $B \sim 10^{-3}\,\mathrm{G}$ for electrons around a $10\,M_\odot$ black hole. This motivates a detailed study of charged-particle dynamics around a black hole surrounded by anisotropic matter and immersed in a uniform magnetic field, as described by the four-vector potential (5) and (6). Particular emphasis is placed on the observational signatures of the anisotropy parameter K and the magnetic coupling parameter Ω_B, as well as on their potential degeneracy with the Kerr spin parameter a.

We consider the motion of a charged particle in the vicinity of a central compact object. For such systems, the Hamilton-Jacobi formalism provides a convenient description of the dynamics of particles orbiting central masses. In the presence of an external electromagnetic field, the equation reads

$$g^{\alpha\beta}\left(\frac{\partial S}{dx^{\alpha}} + eA_{\alpha}\right)\left(\frac{\partial S}{dx^{\beta}} + eA_{\beta}\right) = -m^2, \tag{8}$$

where e and m denote the electric charge and rest mass of the particle, respectively.

In general, Eq. (8) does not admit a separable solution when the system is non-integrable. In such cases, the dynamics are more conveniently described using a Hamiltonian framework [43–48]. However, when the motion is confined to the equatorial plane, the presence of the Killing variables t and φ allows Eq. (8) to be written

CPC Accepted

in the following separable form:

$$\mathcal{S} = -Et + L\varphi + \mathcal{S}_r + \mathcal{S}_\theta \,, \tag{9}$$

where E and L denote the energy and angular momentum of the test particle, respectively. The equation of motion can then be rewritten as follows:

$$-\frac{\mathcal{E}^2}{1-\frac{2M}{r}-\frac{K}{r^{2\omega}}}+\left(1-\frac{2M}{r}-\frac{K}{r^{2\omega}}\right)\left(\frac{\partial \mathcal{S}}{\partial r}\right)^2+ \\ +\frac{1}{r^2}\left(\frac{\partial \mathcal{S}}{\partial \theta}\right)^2+\frac{\left(\mathcal{L}+eA_\varphi\right)^2}{r^2\sin^2\theta}=-1. \tag{10}$$

Here, $\mathcal{E}=E/m$ and $\mathcal{L}=L/m$ denote the specific energy and specific angular momentum of the test particle, respectively. The effective potential for the test particle can be derived from the equations of motion and, for motion in the equatorial plane ($\theta=\pi/2$), takes the following form:

$$\dot{r}^2 = \mathcal{E}^2 - V_{\rm eff}, \tag{11}$$

which, for $\omega = 1/3$ reads

$$V_{\rm eff} = \left(1-\frac{2M}{r}-\frac{K}{r^{2\omega}}\right)\times \\ \times\left[1+\frac{\left(\mathcal{L}+\Omega_B r^2\left(1+\frac{K(1-2\omega)}{2\omega(1+2\omega)}\,r^{-2\omega}\right)\right)^2}{r^2}\right]. \tag{12}$$

and, for $\omega = 0$,

$$V_{\rm eff} = \left(1-\frac{2M}{r}-K\right)\times \\ \times\left[1+\frac{\left(\mathcal{L}+\Omega_B r^2\left(1-K\log\frac{r}{M}\right)\right)^2}{r^2}\right]. \tag{13}$$

The cyclotron frequency of a charged particle, defined as $\Omega_B = eB/(2m)$, characterizes the frequency of the particle's motion induced by the coupling between its electric charge and the external magnetic field. Here, Ω_B is treated as a free coupling parameter whose sign reflects the relative orientation of the particle charge and the magnetic field at the single-particle level, rather than a property of a specific astrophysical plasma configuration. Because realistic accretion plasmas are globally neutral, both signs are, in principle, realized simultaneously by different charge species within the same field. A consistent determination of the physically dominant regime would therefore require a magnetohydrodynamic treatment of the surrounding plasma, which lies beyond the scope of the present test-particle analysis.

Fig. 2 shows the effective potential governing the radial motion of a charged test particle with angular momentum $\mathcal{L}=6$, obtained using the corrected Wald potential (7). This potential was constructed by extending Wald's method [23] to this non-Ricci-flat background, following Ref. [49]. In the upper panels, where the two anisotropic curves have the same value $\Omega_B = 0.03$, increasing K from 0.05 to 0.1 lowers both the potential barrier and the potential well. For dust, this effect is mainly due to the asymptotic factor $1-K$ in $f(r)$, and the minimum shifts outward. For radiation, the effect is much weaker. The Schwarzschild reference curve is plotted without a magnetic field; therefore, at large radii it lies below the magnetized curves, whose growth is driven by the magnetic confinement term $\propto \Omega_B^2 r^2$. In the lower panels, a negative Ω_B lowers the potential and deepens the well, thereby strengthening the particle's binding, whereas a positive Ω_B raises the potential and weakens the binding. Because $V_{\rm eff}$ is invariant under $(\mathcal{L},\Omega_B)\to(-\mathcal{L},-\Omega_B)$, the sign of Ω_B is meaningful only relative to the orbital motion; we take $\mathcal{L}>0$ throughout. This behavior is consistent with the ISCO and efficiency results discussed in Sec. III, where negative Ω_B moves the ISCO toward the horizon and increases η. The strong sensitivity of the effective potential and orbital structure to the magnetic coupling is consistent with earlier studies of charged particle dynamics around magnetized black holes [50–52].

For circular motion of the test particle in the equatorial plane, one can impose the following conditions:

$$\dot{r} = 0 \,, \quad V'_{\rm eff}(r) = 0 \,. \tag{14}$$

In all cases presented in this figure, the main trend is that the orbital energy $\mathcal{E}$ increases steeply at small radii and reaches a minimum at a certain distance. The results demonstrate that both the deviation parameter K and the magnetic parameter Ω_B significantly influence the orbital dynamics of test particles. Increasing K leads to higher orbital energy at small radii around the central black hole in both the radiation and dust cases, whereas in the dust case the orbital energy becomes lower at larger radii. A comparison of the cases $\omega = 0$ and $\omega = \frac{1}{3}$ indicates that, at large distances, the latter asymptotically recovers the Schwarzschild black hole limit. The sign of the magnetic parameter also plays a crucial role: a positive Ω_B makes the orbits more energetically demanding, whereas a negative Ω_B shifts the particle orbits closer to the central object. Consequently, the stable dynamics of charged particles in the vicinity of the black hole is governed by a delicate interplay between gravitational and electromagnetic effects.

Given the specific energy, the relationship between

CPC Accepted

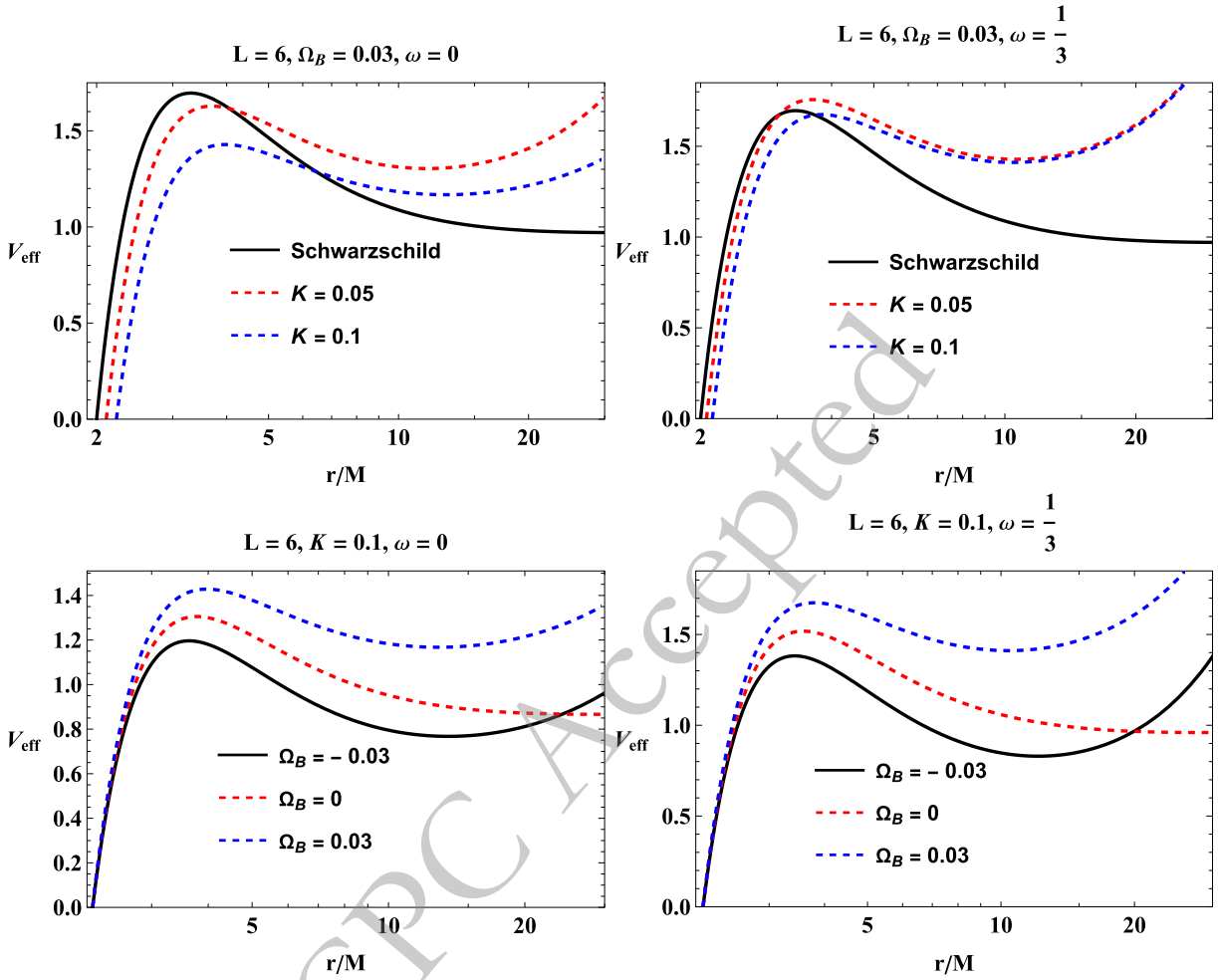
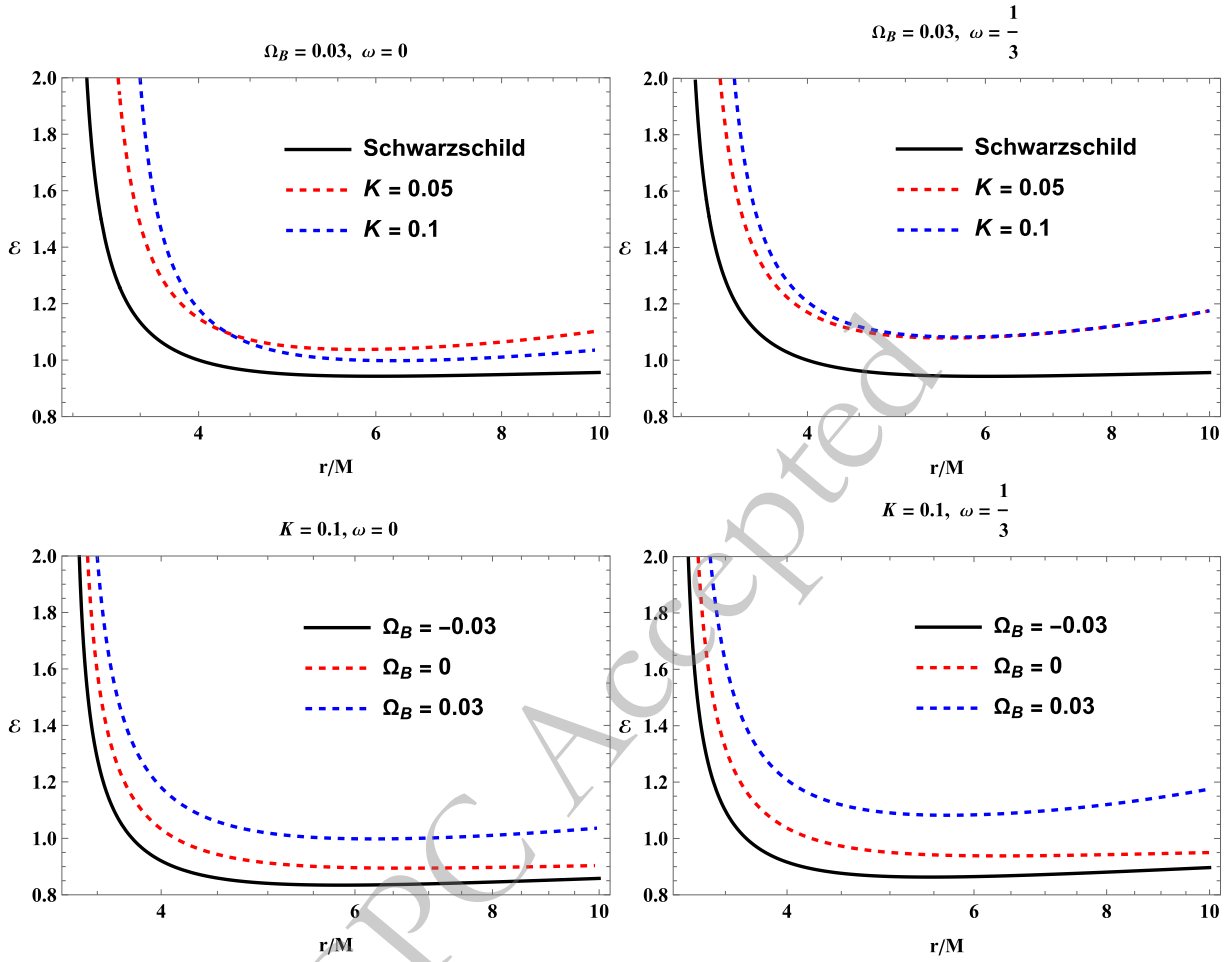


Fig. 2. (color online) Effective potential as a function of the radial coordinate r for $M = 1$. The upper panels show the dependence on the anisotropy parameter, whereas the lower panels show the dependence on the magnetic interaction parameter ($\Omega_B = eB/(2m)$). For reference, we also include the Schwarzschild black hole result in the absence of a magnetic field, shown by the solid black line in the upper panels.

the energy and the radius of the circular orbit of a test particle can be derived directly from these conditions, as shown in Fig 3. In the upper panels, each curve decreases steeply near the last stable radius, reaches a shallow minimum, and then increases gradually outward. Raising K shifts the entire profile above the vacuum reference in both matter models, indicating that more energy is required to maintain a circular orbit at any given radius, while the minimum moves slightly outward as the binding weakens. For dust, the offset introduced by larger K remains nearly constant out to the largest radii plotted. For radiation, the two anisotropic curves instead converge and turn upward at large distances. In the lower panels, varying Ω_B produces the opposite trend to K: a negative coupling lowers the orbital energy at every radius and favors more tightly bound orbits, whereas a positive coupling raises it and makes circular motion progressively more energetically costly. At large radii, the two matter models differ: the positive-coupling curve rises more steeply for radiation than for dust, so the spread among the curves widens more visibly in the $\omega = 1/3$ panel.

The angular momentum of a charged test particle exhibits a radial dependence, as illustrated in Fig 4. The upper panels show that a larger K increases $\mathcal{L}/M$ near the black hole for both the dust and radiation cases. The deviation from the Schwarzschild reference also increases toward the outer edge of the plotted range, slightly more in the radiation case than in the dust case. The lower panels show that a positive coupling increases the angular momentum threshold for stable circular motion near the ISCO, whereas a negative coupling decreases it, allowing stable orbits closer to the black hole. However, this ordering breaks down at larger radii, where the $\Omega_B = -0.03$ curve crosses above the $\Omega_B = 0$ curve. Thus, the sign of Ω_B does not determine the ordering of the angular momentum across the full orbital range.

CPC Accepted



CPC Accepted

Fig. 3. (color online) Radial dependence of the specific orbital energy of a test particle for different values of the anisotropy parameter (upper panels) and magnetic interaction (lower panels) for two values of ω. For reference, we also include the Schwarzschild black hole result in the absence of a magnetic field, indicated by the solid black line (upper panels).

III. ISCO ANALYSIS AND ISCO-BASED DEGENERACY WITH THE KERR SPIN

Using these results, we now investigate whether the parameters Ω_B and K can reproduce the ISCO radius and efficiency associated with the Kerr spin parameter a. The central idea is that, if such a degeneracy exists, then, for a given ISCO radius, a constraint relating the Kerr spin parameter a to the anisotropy and magnetic-field parameters can be established. In other words, a black hole with nonzero K and Ω_B could reproduce the same ISCO radius as a rotating Kerr black hole with spin a. As a preliminary step, we examine the functional dependence of the ISCO radius on the parameters of interest. To facilitate this analysis, we impose an additional condition in conjunction with Eq. (14).

$$V''_{\rm eff}(r) = 0\,. \tag{15}$$

Using these three conditions together with Eqs. (14)–(15), a plot can be constructed to illustrate the dependence of the ISCO radius on the parameters K and Ω_B, as shown in Fig. 5.

Fig. 5 shows that increasing the anisotropy parameter K enlarges the ISCO radius (upper panels), a trend qualitatively reminiscent of the effect of the spin parameter a on retrograde orbits in the Kerr spacetime. However, this growth does not follow a fixed ordering with respect to Ω_B throughout the parameter range. In the dust case, the curves for $\Omega_B = 0$ and $\Omega_B = 0.03$ intersect near $K \approx 0.18$ and subsequently exchange order, whereas in the radiation case no such crossing is observed within the narrower range of K considered.

The lower panels of Fig. 5, which show the dependence of $r_{\rm ISCO}$ on Ω_B, exhibit qualitatively different behavior. The ISCO radius attains a maximum near $\Omega_B \approx 0$ and decreases on both sides of this point, with the decline being markedly steeper toward negative values of the magnetic parameter than toward positive ones. This asymmetry becomes more pronounced as K increases,

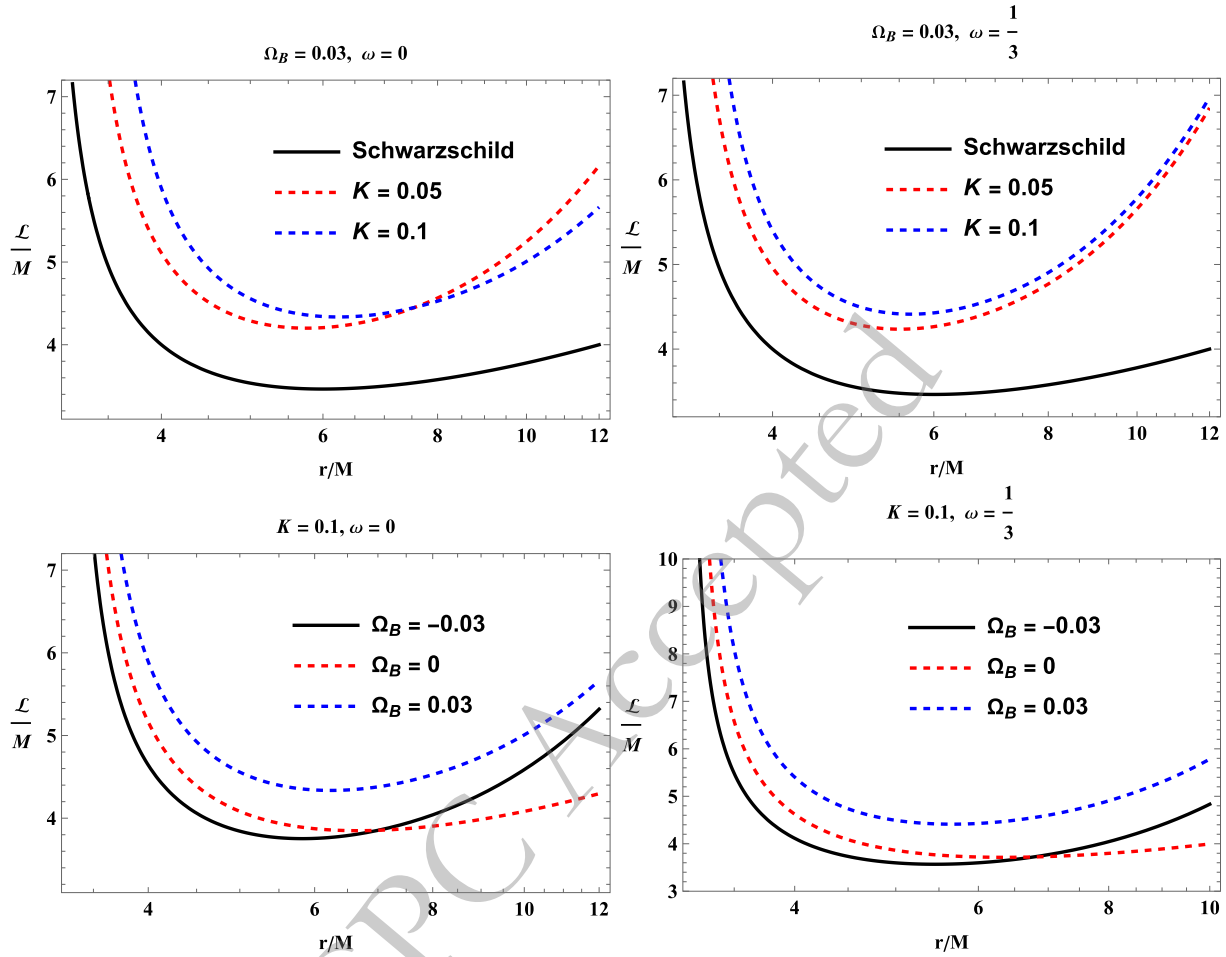


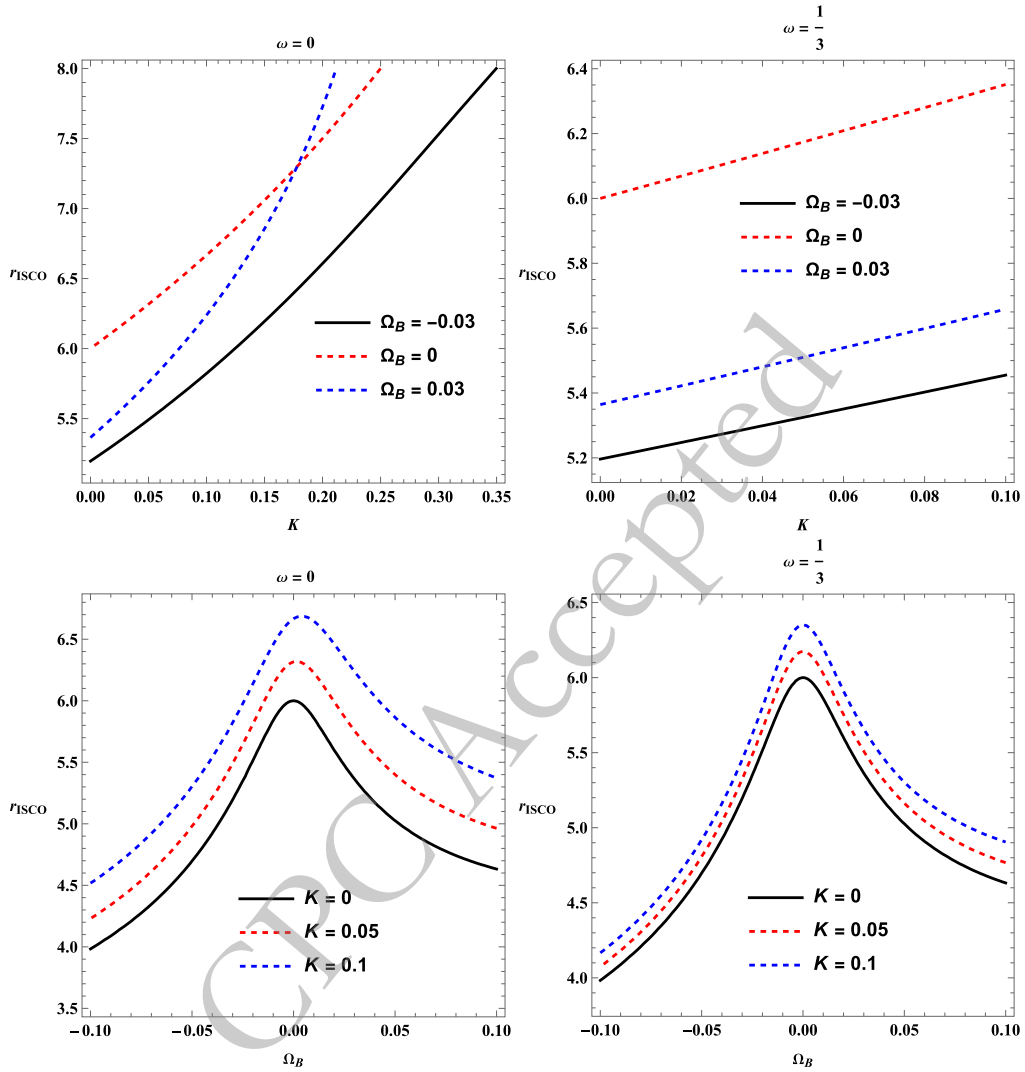
Fig. 4. (color online) Circular-orbit angular momentum evaluated for different values of the anisotropy parameter K, state parameter ω, and magnetic coupling Ω_B.

CPC Accepted

with the $K = 0.1$ curve lying both higher and broader than the $K = 0$ curve. This behavior reflects the fact that the location of the ISCO is governed by the combined effects of gravitational and electromagnetic interactions. Because this combination takes different values on either side of $\Omega_B = 0$, the ISCO location is correspondingly asymmetric with respect to Ω_B. Physically, for $\mathcal{L} > 0$ and negative Ω_B, the Lorentz force acting on the orbiting particle is directed away from the black hole (the anti-Larmor configuration [53]); by partially balancing the gravitational attraction, it allows stable circular orbits closer to the horizon with lower energy, thereby shifting the ISCO inward and enhancing the released binding energy. For positive Ω_B, the Lorentz force is directed toward the black hole (the Larmor configuration), and the inward shift of the ISCO is considerably weaker. A comparison between the dust and radiation cases further shows that the three K curves are considerably more widely separated for $\omega = 0$ than for $\omega = 1/3$, where they nearly coincide. This indicates that the sensitivity of the ISCO radius to the anisotropy parameter K is substantially greater in the dust-dominated regime than in the radiation-dominated one.

Finally, we revisit the question posed at the beginning of this section: to what extent can the parameters K and Ω_B replicate the role of the Kerr rotation parameter a? Recalling the well-established dependence of the ISCO radius in Kerr spacetime on a, one can construct parameter degeneracy curves, as illustrated in Fig. 6, for matching the ISCO radius in the two black hole spacetimes.

Fig. 6 presents degeneracy maps in the parameter space of K and Ω_B that yield Kerr-like ISCO radii for two representative values of the state parameter, with the color scale encoding the equivalent Kerr spin parameter $a_{\rm eff}$. In both panels, a narrow horizontal band centered at $\Omega_B \approx 0$ exhibits the lowest values of $a_{\rm eff}$, indicating that a wide range of K can reproduce the ISCO radius of a slowly rotating Kerr black hole when the magnetic coupling is weak. Away from this band, the trend is markedly asymmetric. For negative Ω_B, the transition to red tones is substantially steeper, with $a_{\rm eff}$ reaching values as high



CPC Accepted

Fig. 5. (color online) Dependence of the ISCO radius on the parameter K and the magnetic field parameter Ω_B for two different values of the state parameter ω.

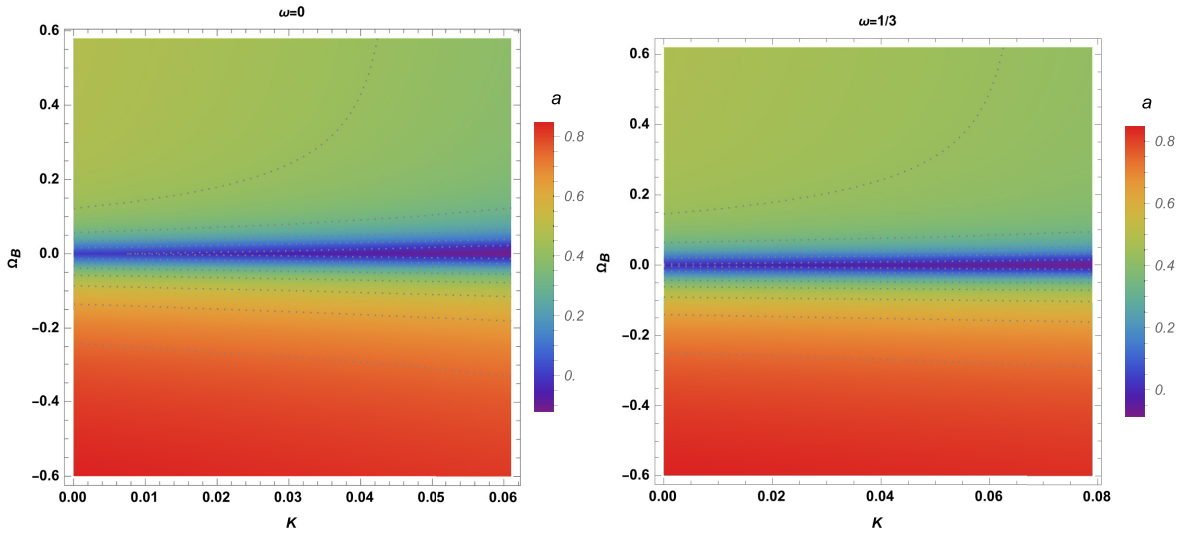


Fig. 6. (color online) Degeneracy plots for the anisotropy parameter K and the magnetic interaction Ω_B that yield Kerr-like ISCO radii for $\omega = 0$ (left) and $\omega = 1/3$ (right).

as $a_{\rm eff} \approx 0.85$ at the most negative couplings considered. By contrast, for positive Ω_B, the color remains in the green range, $a_{\rm eff} \approx 0.48$, even at the largest values plotted. Thus, a negative magnetic coupling corresponds to a much higher Kerr-equivalent spin than a positive coupling of equal magnitude. The contours are nearly horizontal across the full range of K in both panels, confirming that the equivalent spin is determined almost entirely by Ω_B rather than by K. Overall, the map indicates that different combinations of matter density and magnetic field strength can reproduce the same ISCO radius as a Kerr black hole, indicating a degeneracy in the interpretation of black hole spin from accretion-disk observables alone.

A crucial aspect of the mass accretion process is the ability of the central object to convert infalling material into outgoing electromagnetic radiation. The efficiency of this mechanism is defined as the ratio between the flux of photons that successfully escape to infinity from the disk surface and the rate at which mass–energy is absorbed by the central black hole, as discussed in earlier studies [54, 55]. Generally, this efficiency is expressed in terms of the specific energy at the ISCO [56],

$$\eta = 1 - E_{\rm ISCO}. \tag{16}$$

Using the specific energy expression given in Eqs. (11) and (14), the corresponding values of η can be obtained.

Fig. 7 illustrates the dependence of the radiative efficiency η on the anisotropic density parameter K and the magnetic field parameter Ω_B. In both panels, in the absence of a magnetic field, the parameter K has little effect on the radiative efficiency, which remains low. By contrast, the presence of a magnetic field notably increases the efficiency, with $\eta \simeq 0.45$ as Ω_B becomes more negative, because enhanced magnetic coupling allows particles to release substantially more binding energy at the ISCO. The two panels are evaluated over slightly different ranges of K, differing by 0.02, which reflects the distinct parameter domains admissible for each equation of state.

Comparing the two cases, radiation-dominated matter tends to suppress the efficiency somewhat in the weak-field regime relative to dust. In the strong-field limit, however, this distinction largely disappears, and both cases approach comparably high efficiency. This indicates that, once magnetic coupling becomes dominant, the equation of state of the surrounding matter plays only a secondary role.

This behavior suggests a physical analogy with the Kerr spacetime. Just as increasing spin shifts the ISCO inward and enhances the binding energy released before capture, an increasingly negative value of Ω_B appears to have a qualitatively similar effect on the effective potential governing particle motion near the horizon.

Motivated by this qualitative resemblance to the Kerr spacetime, it is natural to ask whether the radiative efficiency of the present magnetized, anisotropic configuration can be quantitatively mapped to an equivalent Kerr spin parameter. To address this question, we introduce an effective Kerr-equivalent spin $a_{\rm eff}$, obtained by matching the radiative efficiency $\eta(K,\Omega_B)$ to that of a Kerr black hole with spin a, as shown in Fig. 8.

In Fig. 8, the color scale denotes the Kerr-equivalent spin parameter $a_{\rm eff}$, defined by matching the radiative efficiency of a black hole surrounded by anisotropic matter and immersed in an external magnetic field (see Eq. (16)) to that of the Kerr spacetime.

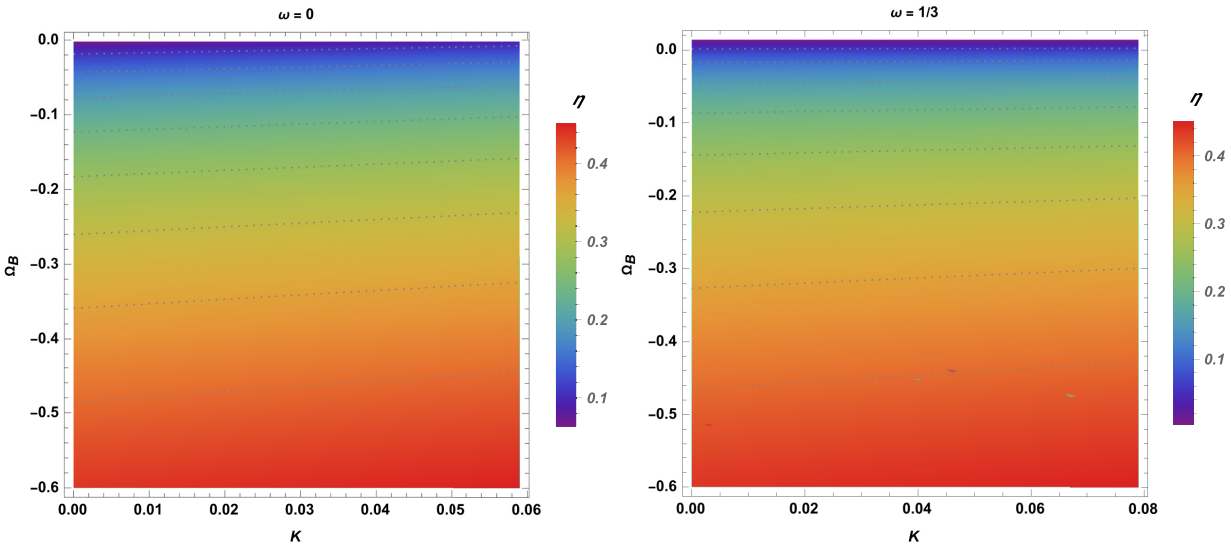


Fig. 7. (color online) Dependence of the radiative efficiency η on the anisotropic density parameter K and magnetic-field parameter Ω_B.

CPC Accepted

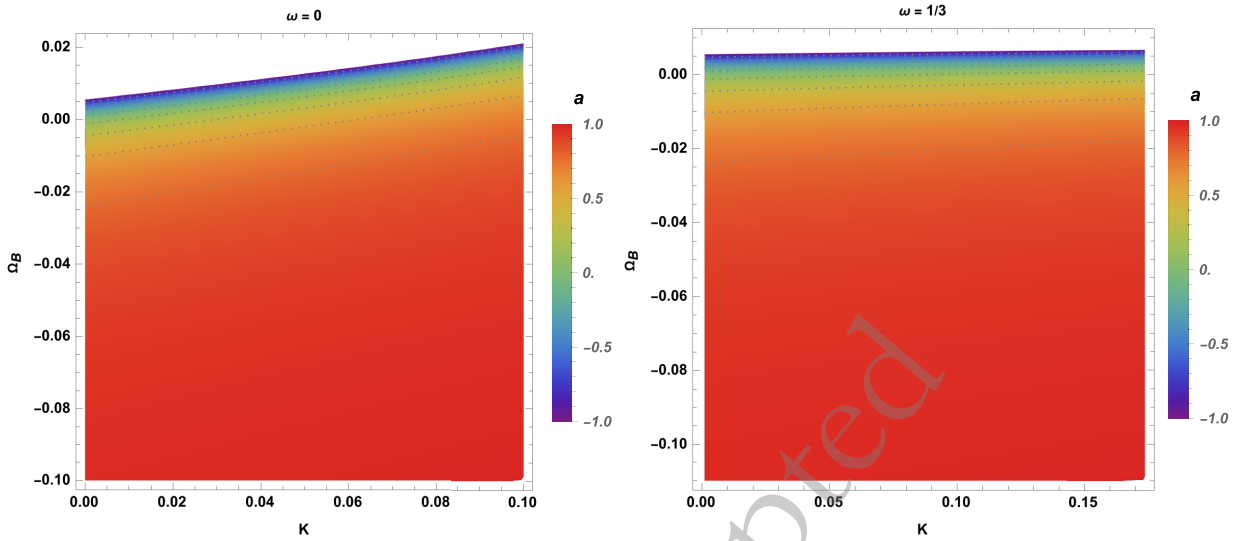


Fig. 8. (color online) Degeneracy plots for matched radiative efficiency.

$$\eta_{\rm Kerr} = 1 - E^{\rm Kerr}_{\rm ISCO}(a). \tag{17}$$

This relation defines an effective Kerr spin $a_{\rm eff}$ such that

$$\eta(K,\Omega_B) = \eta_{\rm Kerr}(a_{\rm eff}). \tag{18}$$

In both panels, the effective spin parameter varies primarily along the Ω_B direction, indicating that magnetic-field coupling is the primary driver of Kerr-like behavior. A narrow region near $\Omega_B \gtrsim 0$ exhibits blue–purple tones, corresponding to small or negative values of $a_{\rm eff}$. It transitions through green tones near $\Omega_B \approx 0$, corresponding to Schwarzschild-like behavior ($a_{\rm eff} \approx 0$). By contrast, increasingly negative values of Ω_B produce a rapid transition to yellow–red colors, indicating larger positive Kerr-equivalent spins. This trend shows that sufficiently strong magnetic fields in the negative-Ω_B regime enhance gravitational binding at the ISCO and can reproduce radiative efficiencies typical of rapidly rotating Kerr black holes.

The dependence on the anisotropic density parameter K is comparatively weaker, as reflected by the nearly horizontal color gradients and only mild inclinations of the degeneracy contours. Nevertheless, a systematic tilt is visible, implying that increasing K shifts the efficiency degeneracy toward less negative values of Ω_B. In particular, for the dust case, the influence of K is significantly stronger than for the radiation case, and increasing K at fixed Ω_B yields higher Kerr-equivalent spin values. Most importantly, the plots show that a broad range of Kerr-equivalent spins can be reproduced for both values of ω through appropriate combinations of K and Ω_B. However, as noted above, the accessible range of $a_{\rm eff}$ is markedly wider for negative Ω_B than for positive Ω_B.

Overall, the figure demonstrates that a broad region of the parameter space reproduces the same radiative efficiencies as in the Kerr spacetime, revealing a pronounced degeneracy in the ISCO-based radiative efficiency between non-rotating magnetized black holes surrounded by anisotropic matter and genuinely spinning Kerr black holes.

IV. CONCLUSION

In this paper, we explored the dynamics of charged test particles around a non-rotating black hole surrounded by anisotropic matter and immersed in an external magnetic field, with the aim of clarifying whether such a system can reproduce the ISCO radius and the ISCO-based radiative efficiency of a Kerr black hole. Employing the Hamilton-Jacobi formalism, we performed a systematic analysis of the effective potential, circular orbits, ISCO properties, and radiative efficiency, explicitly accounting for the combined effects of the anisotropy parameter K, the equation-of-state parameter ω, and the magnetic coupling Ω_B.

Our study demonstrates that the dynamics of charged test particles around non-rotating black holes immersed in anisotropic matter and external magnetic fields are governed by a subtle interplay among the matter density parameter K, the matter state parameter ω, and the magnetic parameter Ω_B. The horizon radius is sensitive to the matter state; for the same K, radiation produces systematically smaller horizons than dust, highlighting the influence of the effective matter field. At fixed angular momentum, increasing K lowers the effective potential, mainly in the dust case. In the region of the potential barrier and well, negative Ω_B lowers the potential and strengthens the binding, whereas positive Ω_B raises it, in agreement with the behavior of the ISCO and the radiative efficiency. Orbital energy and angular momentum

CPC Accepted

both increase near the black hole as K increases, while at larger radii the dust case exhibits lower orbital energy and angular momentum than the radiation case. The magnetic parameter plays a crucial role: positive Ω_B increases the energy and angular-momentum requirements for stable orbits, whereas negative Ω_B shifts orbits inward, enhancing gravitational binding and modifying the location of stable circular orbits.

The ISCO radius exhibits a monotonic increase with K, resembling the effect of the Kerr spin parameter a, indicating that, as far as the ISCO radius is concerned, K can partly play the role of the spin parameter in non-rotating backgrounds. Radiation-dominated environments reduce the overall ISCO radius, yet the trend with K persists, confirming its robustness. The ISCO location is asymmetric with respect to the magnetic field, with negative Ω_B producing more rapid inward shifts, particularly at larger K, revealing a strong coupling between the magnetic field and the matter distribution. Degeneracy maps in the K and Ω_B parameter space show that multiple combinations of density and magnetic parameters can reproduce Kerr-like ISCO radii for both dust and radiation cases, illustrating a potential degeneracy in interpreting spin from accretion-disk observations.

Radiative efficiency η is predominantly controlled by Ω_B and increases to $\eta \approx 0.45$ at large negative Ω_B, a value comparable to, and even slightly above, the maximal value $\eta = 1 - 1/\sqrt{3} \simeq 0.42$ of an extremal Kerr black hole. The density parameter K mainly affects the background geometry and exerts a weaker influence on the efficiency, although in the dust case increasing K at fixed Ω_B yields higher Kerr-equivalent spins. Effective spin maps further confirm that a broad range of Kerr-equivalent spins can be reproduced, although the accessible range is markedly wider for negative Ω_B (reaching $a_{\rm eff} \gtrsim 0.85$) than for positive Ω_B (limited to $a_{\rm eff} \approx 0.5$) for both values of ω, with the magnetic field acting as the primary driver of Kerr-like behavior and K providing a secondary tuning effect.

Overall, our results reveal a pronounced degeneracy, at the level of the ISCO radius and radiative efficiency, between non-rotating magnetized black holes surrounded by anisotropic matter and spinning Kerr black holes. This degeneracy holds robustly over an extended region of the (K,Ω_B) plane, although its strength and the accessible range of $a_{\rm eff}$ depend asymmetrically on the sign of Ω_B, emphasizing that environmental effects, including anisotropic matter and magnetic interactions, must be carefully accounted for when interpreting black hole spin from X-ray disk-based observations. This study provides a framework for understanding how non-rotating black holes in realistic astrophysical environments can reproduce the ISCO-based and efficiency-based observational signatures associated with rotation, with potential implications for accretion physics, jet formation, and X-ray-based black hole spin measurements. We note that the degeneracy identified here is restricted to the ISCO radius and the ISCO-based radiative efficiency. Since, in the test-field approximation, null geodesics do not depend on Ω_B, the shadow of the present configuration is circular and is determined by K and ω alone. It is therefore expected to differ from the shadow of a Kerr black hole with the same ISCO radius, so horizon-scale imaging offers a natural way to break the degeneracy found here. A quantitative shadow analysis, together with other signatures of the Kerr spacetime, such as frame-dragging effects, photon ring displacement, and image asymmetry, as well as a Novikov–Thorne treatment of a magnetized disk, will be the subject of future work.

CPC Accepted

References

[1] A. Abdujabbarov, B. Toshmatov, Z. Stuchlík, and B. Ahmedov, Int. J. Mod. Phys. D **26**, 1750051 (2017)

[2] Event Horizon Telescope Collaboration, Astrophysical Journal Letters **875**, L1 (2019), arXiv: 1906.11238[astro-ph.GA]

[3] J. M. Bardeen, W. H. Press, and S. A. Teukolsky, Astrophysical Journal **178**, 347 (1972)

[4] C. Bambi, *Black Holes: A Laboratory for Testing Strong Gravity* (Springer, Singapore, 2017).

[5] T. Johannsen, Classical and Quantum Gravity **33**, 124001 (2016)

[6] R. A. Konoplya and A. Zhidenko, Reviews of Modern Physics **83**, 793 (2011)

[7] N. Heidari, A. A. A. Filho, R. C. Pantig, and A. Övgün, arXiv preprint **2024**, arXiv:2410.08246 (2025), arXiv:2410.08246[gr-qc].

[8] D. Psaltis, Living Reviews in Relativity **11**, 9 (2008)

[9] V. Cardoso, E. Franzin, and P. Pani, Physical Review Letters **116**, 171101 (2016)

[10] K. A. Bronnikov and O. B. Zaslavskii, Phys. Rev. D **84**, 084013 (2011), arXiv: 1107.4701[gr-qc]

[11] L. Herrera and N. O. Santos, Phys. Rep. **286**, 53 (1997)

[12] I. Cho and H.-C. Kim, Chinese Physics C **43**, 025101 (2019), arXiv: 1703.01103[gr-qc]

[13] M. S. Morris and K. S. Thorne, Am. J. Phys. **56**, 395 (1988)

[14] H.-C. Kim, B.-H. Lee, W. Lee, and Y. S. Myung, Phys. Rev. D **101**, 064067 (2020), arXiv: 1912.09709[gr-qc]

[15] B.-H. Lee, W. Lee, and Y. S. Myung, Phys. Rev. D **103**, 064026 (2021), arXiv: 2101.04862[gr-qc]

[16] A. Ghosh and U. Debnath, arXiv preprint **2025**, arXiv:2506.15240 (2025), arXiv:2506.15240[gr-qc].

[17] J. Rayimbaev, A. Abdujabbarov, M. Jamil, and W.-B. Han, Nuclear Physics B **966**, 115364 (2021), arXiv: 2009.04898[gr-qc]

[18] Z. Stuchlík and J. Vrba, arXiv preprint **2021**, arXiv:2110.07411 (2021), arXiv:2110.07411[astro-ph.HE].

[19] Y. Feng, A. Ashraf, S. Mumtaz, S. K. Maurya, G. Mustafa, and F. Atamurotov, Journal of High Energy Astrophysics **43**, 158 (2024)

[20] A. Çalışkan, G. Mustafa, T. Naseer, S. K. Maurya, E.

Güdekli, S. Murodov, and F. Atamurotov, Journal of High Energy Astrophysics **44**, 99 (2024)
[21] M. Zajaček, A. Tursunov, A. Eckart, *et al.*, arXiv preprint (2018), arXiv:1812.03574[astro-ph.GA].
[22] M. D. Johnson, V. L. Fish, S. S. Doeleman, *et al.*, arXiv preprint (2015), arXiv:1512.01220[astro-ph.HE].
[23] R. M. Wald, Phys. Rev. D **10**, 1680 (1974)
[24] Event Horizon Telescope Collaboration, Astrophys. J. Lett. **964**, L25 (2024)
[25] B. Narzilloev, D. Malafarina, A. Abdujabbarov, and C. Bambi, Eur. Phys. J. C **80**, 784 (2020), arXiv: 2003.11828[gr-qc]
[26] B. Narzilloev, D. Malafarina, A. Abdujabbarov, B. Ahmedov, and C. Bambi, Phys. Rev. D **104**, 064016 (2021), arXiv: 2105.09174[gr-qc]
[27] B. Narzilloev, I. Hussain, A. Abdujabbarov, and B. Ahmedov, Eur. Phys. J. Plus **137**, 645 (2022), arXiv: 2205.11760[gr-qc]
[28] B. Narzilloev and B. Ahmedov, New Astron. **98**, 101922 (2023)
[29] B. Narzilloev and B. Ahmedov, Int. J. Mod. Phys. A **38**, 2350026 (2023)
[30] H. Alibekov, B. Narzilloev, A. Abdujabbarov, and B. A, Symmetry **15** (2023), 10.3390/sym15071414.
[31] A. Davlataliev, B. Narzilloev, I. Hussain, A. Abdujabbarov, and B. Ahmedov, Phys. Dark Univ. **42**, 101340 (2023)
[32] A. Davlataliev, B. Narzilloev, I. Hussain, A. Abdujabbarov, and B. Ahmedov, Phys. Dark Univ. **46**, 101569 (2024)
[33] A. N. Aliev and N. Özdemir, Mon. Not. R. Astron. Soc. **336**, 241 (2002)
[34] B. Saidov, B. Narzilloev, A. Abdujabbarov, M. Khudoyberdieva, and B. Ahmedov, Universe **10**, 454 (2024)
[35] J. Rayimbaev, A. Demyanova, U. Camci, A. Abdujabbarov, and B. Ahmedov, International Journal of Modern Physics D **30**, 2150019 (2021), arXiv: 2010.04969[gr-qc]
[36] M. Kološ, M. Shahzadi, and A. Tursunov, Eur. Phys. J. C **83**, 323 (2023)
[37] S. Kenzhebayeva, S. Toktarbay, A. Tursunov, and M. Kološ, Phys. Rev. D **109**, 063005 (2024)
[38] C. Li, P. Zhang, *et al*., Eur. Phys. J. C **82**, 494 (2022)
[39] V. V. Kiselev, Classical and Quantum Gravity **20**, 1187 (2003), arXiv: gr-qc/0210040[gr-qc]
[40] S. Shaymatov, D. Malafarina, and B. Ahmedov, Physics of the Dark Universe **34**, 100891 (2021)
[41] M. Boltatoshova, B. Narzilloev, and B. Ahmedov, Communications in Theoretical Physics **77**, 085403 (2025)
[42] A. Abdujabbarov, B. Ahmedov, and A. Hakimov, arXiv preprint (2011), arXiv:1101.4741[gr-qc].
[43] M. Kološ, Z. Stuchlík, and A. Tursunov, Classical and Quantum Gravity **32**, 165009 (2015), arXiv: 1506.06799[gr-qc]
[44] M. Takahashi and H. Koyama, The Astrophysical Journal **693**, 472 (2009), arXiv: 0807.0277[astro-ph]
[45] O. Kopáček, V. Karas, J. Kovář, and Z. Stuchlík, Astrophys. J. **722**, 1240 (2010), arXiv: 1008.4650[astro-ph.HE]
[46] O. Kopáček and V. Karas, Astrophys. J. **787**, 117 (2014), arXiv: 1404.5495[astro-ph.HE]
[47] D. Li and X. Wu, Eur. Phys. J. Plus **134**, 96 (2019), arXiv: 1803.02119[gr-qc]
[48] M. Yi and X. Wu, Phys. Scr. **95**, 085008 (2020)
[49] M. Azreg-Aïnou, The European Physical Journal C **76**, 414 (2016), arXiv: 1603.07894[gr-qc]
[50] X. Sun, X. Wu, Y. Wang, C. Deng, B. Liu, and E. Liang, Universe **7**, 410 (2021)
[51] A. Davlataliev, B. Narzilloev, I. Hussain, A. Abdujabbarov, and B. Ahmedov, The European Physical Journal C **84**, 694 (2024)
[52] S. U. Khan and Z.-M. Chen, The European Physical Journal C **83**, 704 (2023)
[53] V. P. Frolov and A. A. Shoom, Phys. Rev. D **82**, 084034 (2010), arXiv: 1008.2985[gr-qc]
[54] I. D. Novikov and K. S. Thorne, in *Les Houches Summer School of Theoretical Physics: Black Holes* (1973) pp. 343–550.
[55] D. N. Page and K. S. Thorne, Astrophys. J. **191**, 499 (1974)
[56] K. S. Thorne, Astrophysical Journal, Vol. 191, pp. 507-520 (1974) **191**, 507 (1974).

CPC Accepted